Available online at www.sciencedirect.com
ScienceDirect
Journal of Solid State Chemistry 180 (2007) 1934–1942
JOURNAL OF SOLID STATE CHEMISTRY
www.elsevier.com/locate/jssc

Structural studies on a high-pressure polymorph of $NaYSi_2O_6$

Volker Kahlenberg*, Jürgen Konzett, Reinhard Kaindl

Institute of Mineralogy and Petrography, University of Innsbruck, Innrain 52, A-6020 Innsbruck, Austria

Received 19 March 2007; received in revised form 24 April 2007; accepted 30 April 2007
Available online 6 May 2007

Abstract

High-pressure synthesis experiments in the system Na_2O–Y_2O_3–SiO_2 revealed the existence of a previously unknown polymorph of $NaYSi_2O_6$ or $Na_3Y_3[Si_3O_9]_2$ which was quenched from 3.0 GPa and 1000 °C. Structural investigations on this modification have been performed using single-crystal X-ray diffraction data collected at ambient conditions. Furthermore, unpolarized micro-Raman spectra have been obtained from single-crystal material. The high-P modification of $NaYSi_2O_6$ crystallizes in the centrosymmetric space group $C2/c$ with 12 formula units per cell ($a = 8.2131(9)$ Å, $b = 10.3983(14)$ Å, $c = 17.6542(21)$ Å, $\beta = 100.804(9)°$, $V = 1481.0(3)$ Å^3, $R(|F|) = 0.033$ for 1142 independent observed reflections) and belongs to the group of cyclo-silicates. Basic building units are isolated three-membered $[Si_3O_9]$ rings located in layers parallel to (010). Within a single layer the rings are concentrated in strings parallel to [100]. The sequence of directedness of up (U) or down (D) pointing tetrahedra of a single ring is UUU or DDD, respectively. Stacking of the layers parallel to b results in the formation of a three-dimensional structure in which yttrium and sodium cations are incorporated for charge compensation. In more detail, four non-tetrahedral cation positions can be differentiated which are coordinated by 6 and 8 oxygen ligands. Refinements of the site occupancies did not reveal any indication for mixed Na–Y populations on these positions. Finally, several geometrical parameters of rings occurring in cyclo-trisilicate structures have been compiled and are discussed.

Keywords: $NaYSi_2O_6$; Sodium yttrium silicate; High-pressure phase; Polymorphism

1. Introduction

For the silicates with general composition $NaXSi_2O_6$ (X: trivalent cation), many different natural and synthetic representatives can be found. Almost all of these compounds are members of a family of chain structures named after the important rock-forming pyroxene mineral group, including X-cations such as Sc, Ti, V, Cr, Al, In, Fe and Ga [1]. Like scandium, yttrium belongs to the sub-group III of the periodic table of the elements, having similar electronic configurations in the outer-most electronic shell. Therefore, it is not surprising that the oxide crystal chemistry of Sc^{3+} and Y^{3+} is comparable [2,3]. One could thus hypothesize that the corresponding sodium yttrium silicate should adopt or be at least somehow related to the pyroxene structure type.

The existence of the compound $NaYSi_2O_6$ was demonstrated by Cervantes Lee [4] who reported the incongruent melting behavior and an X-ray powder diffraction pattern. Redhammer and Roth [5] tried to synthesize $NaYSi_2O_6$ single crystals using Na_2MoO_4 high-temperature solutions. However, under their experimental conditions this phase was not stable. Only recently the crystal structure of $NaYSi_2O_6$ has been determined from laboratory X-ray powder diffraction data using polycrystalline material prepared by solid-state reactions [6]. According to this study, $NaYSi_2O_6$ forms a tetrahedral chain structure, but the chain architecture differs from the one observed in pyroxenes: whereas the pyroxene family is characterized by slightly corrugated *zweier* single chains, the crystal structure of $NaYSi_2O_6$ contains *vierer* single chains showing a pronounced undulation. Therefore, the question of the existence of a $NaYSi_2O_6$ pyroxene still remains.

The occurrence of pyroxenes like $NaAlSi_2O_6$ (jadeite) in high-pressure metamorphic rocks, e.g., in eclogites, led us

*Corresponding author. Fax: +43 512 507 2926.
E-mail address: volker.kahlenberg@uibk.ac.at (V. Kahlenberg).

0022-4596/$ - see front matter © 2007 Elsevier Inc. All rights reserved.
doi:10.1016/j.jssc.2007.04.021

to the idea that the application of pressure as an additional synthesis parameter may be helpful for the formation of a pyroxene-type modification of $NaYSi_2O_6$. The present paper reports the results of the corresponding first high-pressure experiment.

2. Experimental details

The starting material for the high-P–high-T synthesis of $NaYSi_2O_6$ was made from high-purity ($\geqslant$99.99%) SiO_2, Y_2O_3 and Na_2CO_3 mixed in appropriate proportions by stepwise decarbonation at 700–750 °C with intermittent checks of the loss on ignition. The fired mix was then welded into a 3-mm outer diameter platinum capsule with a length of approximately 6 mm. The high-P–high-T synthesis was performed in an end-loaded Boyd and England-type piston cylinder apparatus [7] using a 1/2″-pressure vessel and a pyrophyllite-BN-NaCl assembly at 1000 °C and 3.0 GPa with a run duration of 123.5 h. The pressure calibration of the piston cylinder is based on the reaction albite $\leftrightarrow$ jadeite + quartz and the α-quartz $\leftrightarrow$ coesite phase transition. The temperature of the experiment was measured with a K-type thermocouple and both pressure and temperature were computer-controlled during the entire run duration.

After quenching to ambient conditions, the crystalline mass was recovered from the capsule and broken into pieces from which several fragments of good optical quality could be obtained. Preliminary investigations included polarized light microscopy indicating an optically biaxial character of the crystals. A part of the sample was used for X-ray powder diffraction verifying the presence of a single phase material. Subsequently, a crystal was mounted on a glass fibre and diffraction data were collected using a Stoe IPDS-2 imaging plate single-crystal diffractometer at ambient conditions. Parameters pertaining to the data collection are summarized in Table 1. The morphology of the fragment was approximated by external faces and an analytical absorption correction based on the indexed faces was applied. Further data reduction included Lorentz and polarization corrections.

Confocal Raman spectra were obtained with a HORIBA JOBIN YVON LabRam-HR 800 Raman micro-spectrometer. Samples were excited at room temperature with the 515 nm emission line of a 30 mW Ar^+ laser through an OLYMPUS 100× objective. The laser spot on the surface had a diameter of approximately 1 μm and a power of about 5 mW. Light was dispersed by a holographic grating with 1800 grooves/mm. Spectral resolution of about 1.8 cm^{-1} was experimentally determined by measuring the Rayleigh line. The dispersed light was collected by a 1024 × 256 open-electrode CCD detector. Confocal pinhole was set to 1000 μm. Spectra were recorded unpolarized. All spectra were baseline-corrected by subtracting line segments and fitted to Gauss–Lorentz functions. Band shifts were calibrated by regularly adjusting the zero-order position of the grating and controlled by measuring the Rayleigh line of a (100) polished single-crystal silicon wafer. Accuracy of Raman band shifts was better than 0.5 cm^{-1}. The detection range was 100–1100 cm^{-1}.

Table 1
Data collection and refinement parameters for high-P $NaYSi_2O_6$

Crystal data	
a (Å)	8.2131(9)
b (Å)	10.3983(14)
c (Å)	17.6542(21)
α (deg)	90
β (deg)	100.804(9)
γ (deg)	90
Volume	1481.0(3) Å^3
Space group	$C2/c$
Z	12
Chemical formula	$NaYSi_2O_6$
Crystal system	Monoclinic
Density (calculated)	3.553 g/cm^3
Absorption coefficient	12.34 mm^{-1}
Intensity measurements	
Crystal shape	Fragment
Crystal size	0.04 × 0.16 × 0.28 mm^3
Diffractometer	Stoe IPDS-II
Monochromator	Graphite
Radiation	Mo$K\alpha$, $\lambda = 0.71073$ Å
X-ray power	50 kV, 40 mA
Detector to sample distance	120 mm
Rotation width in ω	1.5
No. of exposures	120
Irradiation time/exposure	3
Theta range for data collection	2.3–26.7
Index ranges	$-10 \leqslant h \leqslant 10$, $-12 \leqslant k \leqslant 13$, $-22 \leqslant l \leqslant 22$
No. of measured reflections collected	3350
No. of unique reflections	1315
No. of observed reflections ($I > 2\sigma(I)$)	1142
R(int) after absorption correction	0.029
Refinement parameters	
No. of parameters	138
No. of restraints	0
Final R indices [$I > 2\sigma(I)$]	$R_1 = 0.033$, w$R_2 = 0.068$
Final R indices (all data)	$R_1 = 0.042$
Goodness-of-fit on F^2	1.126
Largest diff. peak and hole	0.56 and −0.56 e Å^{-3}

The diffraction symmetry was consistent with the monoclinic Laue group $2/m$. An analysis of the systematic absences pointed to the space groups $C12/c1$ or $C1c1$. Intensity statistics ($\langle |E^2-1| \rangle$) showed only very small deviations from the ideal value for a centrosymmetric distribution. Therefore, structure solution was initiated in space group $C2/c$ using direct methods (program SIR2002 [8]). A partial structure based on the Na and Y ions, the Si atoms and most of the oxygens was found and subsequently completed using difference Fourier synthesis. Scattering curves for neutral atoms were taken from the *International Tables for Crystallography* [9]. The final

Table 2
Atomic coordinates ($\times 10^4$) and equivalent isotropic displacement parameters (Å$^2 \times 10^3$) for high-P $NaYSi_2O_6$

	x	y	z	U(eq)
Y(1)	5000	1069(1)	2500	11(1)
Y(2)	3129(1)	487(1)	4272(1)	10(1)
Si(1)	6354(2)	−1717(2)	3983(1)	10(1)
Si(2)	2337(2)	−1196(2)	2433(1)	10(1)
Si(3)	−58(2)	−1725(2)	3996(1)	11(1)
Na(1)	3217(3)	−3188(3)	4169(1)	26(1)
Na(2)	0	1239(3)	2500	21(1)
O(1)	2856(5)	−41(4)	3023(2)	13(1)
O(2)	7286(5)	2387(4)	2771(2)	14(1)
O(3)	5301(5)	−962(4)	4515(2)	12(1)
O(4)	1578(5)	−1162(4)	4516(2)	12(1)
O(5)	4953(5)	1764(4)	1219(2)	13(1)
O(6)	597(5)	−896(4)	1809(2)	12(1)
O(7)	1684(5)	1601(4)	5568(2)	16(1)
O(8)	6267(5)	−974(4)	3148(2)	13(1)
O(9)	938(5)	1797(4)	3842(2)	14(1)

U(eq) is defined as one third of the trace of the orthogonalized U_{ij} tensor. Y(1) and Na(1) occupy the special Wyckoff site 4*e*. All other atoms reside on general positions.

Table 3
Anisotropic displacement parameters (Å$^2 \times 10^3$)

	U_{11}	U_{22}	U_{33}	U_{23}	U_{13}	U_{12}
Y(1)	9(1)	10(1)	13(1)	0	2(1)	0
Y(2)	8(1)	10(1)	13(1)	0(1)	2(1)	0(1)
Si((1)	9(1)	10(1)	12(1)	1(1)	3(1)	0(1)
Si(2)	7(1)	11(1)	12(1)	−1(1)	2(1)	−1(1)
Si(3)	8(1)	12(1)	14(1)	2(1)	2(1)	−1(1)
Na(1)	18(1)	38(2)	22(1)	7(1)	5(1)	2(1)
Na(2)	24(2)	21(2)	17(2)	0	3(1)	0
O(1)	14(2)	14(2)	11(2)	−2(1)	3(1)	−2(2)
O(2)	13(2)	11(2)	19(2)	0(1)	3(1)	−1(2)
O(3)	11(2)	15(2)	8(2)	−2(1)	0(1)	3(2)
O(4)	9(2)	12(2)	14(2)	2(1)	2(1)	−2(2)
O(5)	13(2)	10(2)	16(2)	0(1)	4(1)	3(2)
O(6)	7(2)	12(2)	16(2)	−2(1)	2(1)	1(2)
O(7)	12(2)	23(2)	12(2)	−1(2)	3(1)	0(2)
O(8)	10(2)	16(2)	11(2)	1(1)	2(1)	1(2)
O(9)	13(2)	9(2)	19(2)	−1(1)	5(1)	−1(2)

The anisotropic displacement factor exponent takes the form: $-2\pi^2[h^2a^*2U_{11} + \cdots + 2hka^*b^*U_{12}]$.

least squares refinement using anisotropic displacement parameters for all atoms was performed with the program SHELXL-97 [10] and converged to a residual $R(|F|) = 0.033$ for 138 parameters for all reflections with $I > 2\sigma(I)$. The largest shift/esd. in the final cycles was <0.001. A summary of the relevant data of the structure determination is given in Table 1. The refined atomic coordinates, equivalent isotropic and anisotropic displacement parameters as well as selected interatomic distances and angles are listed in Tables 2–4, respectively. Figures showing structural details were prepared using the program ATOMS5.1 [11].

Table 4
Selected bond lengths (Å) up to 3.4 Å and angles (deg)

Si(1)–O(9)	1.593(4)	Si(2)–O(2)	1.593(4)
Si(1)–O(3)	1.597(4)	Si(2)–O(1)	1.595(4)
Si(1)–O(8)	1.654(4)	Si(2)–O(6)	1.662(4)
Si(1)–O(7)	1.661(4)	Si(2)–O(8)	1.691(4)
Mean	1.626	Mean	1.635
Si(3)–O(4)	1.590(4)		
Si(3)–O(5)	1.622(4)		
Si(3)–O(6)	1.649(4)		
Si(3)–O(7)	1.667(4)		
Mean	1.632		
Y(1)–O(2)	2.301(4) × 2	Y(2)–O(4)	2.226(4)
Y(1)–O(5)	2.367(4) × 2	Y(2)–O(1)	2.242(3)
Y(1)–O(1)	2.429(4) × 2	Y(2)–O(9)	2.271(4)
Y(1)–O(8)	2.541(4) × 2	Y(2)–O(3)	2.314(4)
		Y(2)–O(3)	2.336(3)
		Y(2)–O(5)	2.347(4)
Na(1)–O(4)	2.394(4)	Na(2)–O(9)	2.420(4) × 2
Na(1)–O(9)	2.411(5)	Na(2)–O(6)	2.624(5) × 2
Na(1)–O(2)	2.515(4)	Na(2)–O(2)	2.650(4) × 2
Na(1)–O(5)	2.565(5)	Na(2)–O(1)	2.704(4) × 2
Na(1)–O(4)	2.634(5)		
Na(1)–O(3)	2.875(5)		
O(9)–Si(1)–O(3)	116.4(2)	O(2)–Si(2)–O(1)	118.3(2)
O(9)–Si(1)–O(8)	110.0(2)	O(2)–Si(2)–O(6)	110.0(2)
O(9)–Si(1)–O(7)	107.8(2)	O(2)–Si(2)–O(8)	114.9(2)
O(3)–Si(1)–O(8)	110.9(2)	O(1)–Si(2)–O(6)	112.6(2)
O(3)–Si(1)–O(7)	105.5(2)	O(1)–Si(2)–O(8)	99.5(2)
O(8)–Si(1)–O(7)	105.5(2)	O(6)–Si(2)–O(8)	99.7(2)
Mean	109.4	Mean	109.2
O(4)–Si(3)–O(5)	114.6(2)	Si(2)–O(6)–Si(3)	122.1(2)
O(4)–Si(3)–O(6)	111.5(2)	Si(1)–O(7)–Si(3)	124.3(2)
O(4)–Si(3)–O(7)	111.6(2)	Si(1)–O(8)–Si(2)	123.7(2)
O(5)–Si(3)–O(6)	108.8(2)		
O(5)–Si(3)–O(7)	105.4(2)		
O(6)–Si(3)–O(7)	104.4(2)		
Mean	109.4		

3. Description of the structure

The crystal structure of the new quenched high-P form of $NaYSi_2O_6$ belongs to the group of cyclo-silicates, i.e., it is not a member of the pyroxene family. Basic building units are three-membered Si_3O_9 rings (see Fig. 1). Therefore, the structural formula could be written as $Na_3Y_3[Si_3O_9]_2$. The rings are concentrated in slightly corrugated layers parallel to (010). Within a single layer the rings are located in rows or bands running parallel to [100] and show a zig–zag-like arrangement. The sequence of directedness of up (*U*) and down (*D*) pointing tetrahedra in the rings can be described as *UUU* or *DDD*. Due to the symmetry requirements of $C2/c$, the directedness of rings belonging to neighboring rows of the same layer is reversed. A projection of the whole structure parallel to [100] and a single layer are given in Figs. 2 and 3. The Si–O distances of the tetrahedra cluster in two groups and follow the expected trend for $[SiO_4]$ groups having two bridging and two terminal atoms:

the distances between the silicon atoms and the six terminal oxygens (O(1), O(2), O(3), O(4), O(5) and O(9)) are considerably shorter (average: 1.598 Å) than the corresponding bond lengths to the bridging oxygens O(6), O(7) and O(8) (average: 1.664 Å). The shortening of the Si–O_{term} bond lengths (by an average of 0.066 Å) results from the stronger attraction between O and Si than between O and the other cations in the structure.

The distortion of the tetrahedra is also reflected in the large spread of the O–Si–O bond angles ranging from 99.5° to 118.3°. Nevertheless, the mean ⟨O–Si–O⟩ angles are close to the ideal value for an undistorted tetrahedron (see Table 4). Numerically, the distortion can be expressed by the quadratic elongations λ and the angle variances σ^2 [12]. The corresponding values for the three crystallographically independent tetrahedra around Si(1)–Si(3) are as follows: $Si(1)O_4$: $\lambda = 1.004$, $\sigma^2 = 17.090$; $Si(2)O_4$: $\lambda = 1.015$, $\sigma^2 = 62.480$; $Si(3)O_4$: $\lambda = 1.004$, $\sigma^2 = 15.591$. The parameters clearly indicate that the $Si(2)O_4$ tetrahedron shows the most pronounced distortion. The Si⋯Si distances of the Si_3O_9 ring in $NaYSi_2O_6$ are 2.951 (Si(1)⋯Si(2)), 2.943

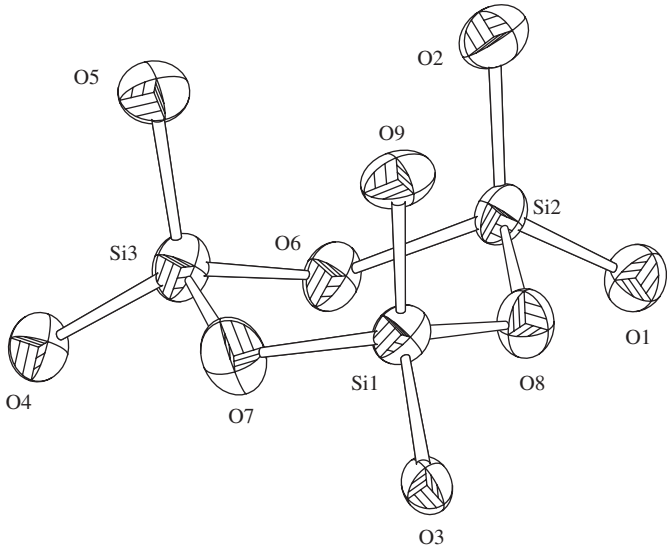

Fig. 1. Side view of the three-membered silicate ring in high-P $NaYSi_2O_6$. Thermal displacement ellipsoids are drawn on the 80% probability level.

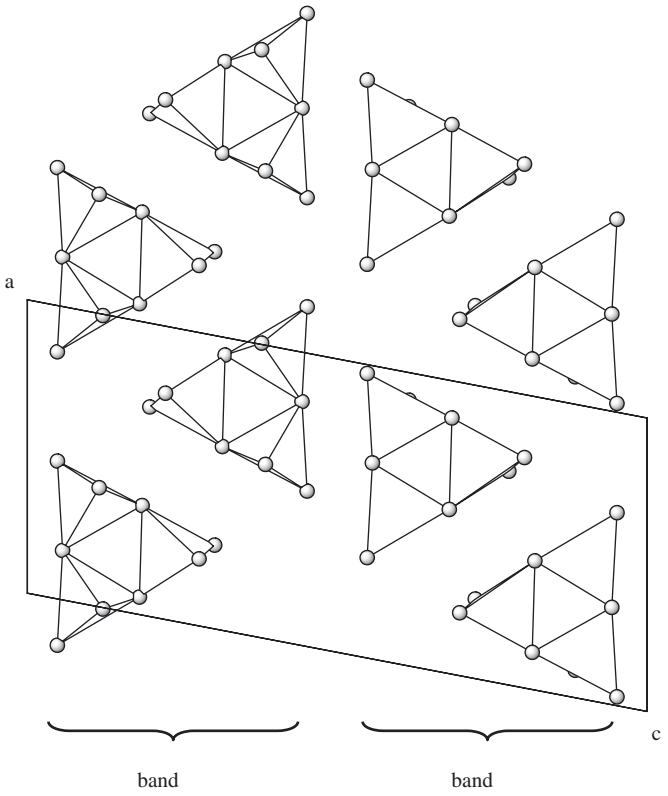

Fig. 3. Single layer parallel to (010) containing three-membered rings. Within the layer the rings are arranged in bands running parallel to [100].

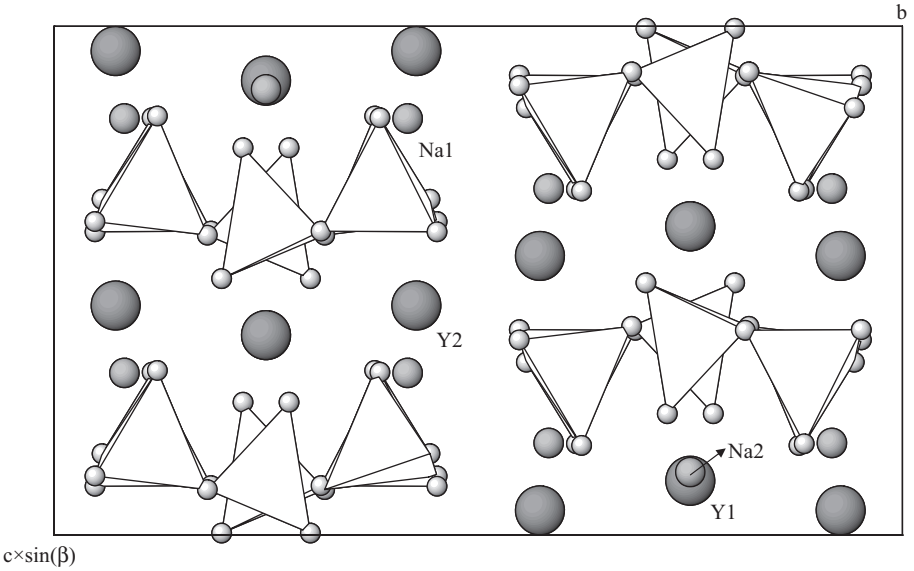

Fig. 2. Projection of the whole structure of high-P $NaYSi_2O_6$ parallel to [100].

(Si(1)···Si(3)) and 2.898 (Si(2)···Si(3)) Å. The corresponding Si–O–Si angles within the rings vary between 122.1° and 124.3°.

Linkage between the cyclic tetrahedral trimers is provided by four symmetrically independent cation positions. Refinements of the site populations did not reveal any evidence for an Na↔Y substitution, i.e., the positions are exclusively occupied by either sodium or yttrium. Y(2) is surrounded by six O atoms in the form of a distorted octahedron. Y(1) and Na(2) in turn have eight nearest oxygen neighbors with irregular coordination polyhedra. The coordination of the Na(1) is less well defined. To an upper limit of 3.0 Å six oxygen ligands can be found (see Table 4). Since typical Na–O bond lengths average at about 2.34 Å [9], the longest Na–O bond at 2.875 Å can be considered extremely weak. Focusing on the inner five oxygen ligands, the coordination sphere could be described as a distorted tetragonal pyramid. A graphical representation of the coordination environments of the Na and Y ions is given in Figs. 4a–d. Apart from Y(2), which connects five different adjacent silicate trimers, the remaining three non-tetrahedral cation sites are linked to four neighboring Si_3O_9 groups.

Bond valence sum (BVS) calculations were performed using the parameter sets for the Si–O, Na–O and Y–O given by Brese and O'Keeffe [13]. The resulting BVS are close to the expected values of +1, +3 and +4, respectively: Na(1): 0.830 v.u.; Na(2): 0.973 v.u.; Y(1): 2.862 v.u.; Y(2): 2.912 v.u.; Si(1): 4.166 v.u.; Si(2): 4.078 v.u. and Si(3): 4.100 v.u. The largest negative deviation (or underbonding) occurs for Na(1) indicating that this sodium cation is exposed to a tensional strain and does not fit so well into the cavities between the tetrahedral rings.

4. Raman spectroscopy

The high-pressure modification of $NaYSi_2O_6$ crystallizes in space group $C2/c$, and its associated factor group is $2/m$. A symmetry analysis using the program Vibratz [14] and the web-based software package of the Bilbao Crystallographic Server [15–17] yields the following theoretical number of vibrational modes:

$$\Gamma_{\mathrm{vib}} = 44A_g + 44B_g + 46A_u + 46A_u.$$

All g-modes are Raman-, all u-modes IR active. The $44A_g$ and B_g modes occur in the spectrum at different polarization geometries of the incident laser and the scattered Raman light. It can be expected that under the unpolarized conditions used in our experiments, A and B modes overlap, resulting in significantly reduced number of bands. We determined 47 bands in the Raman spectrum of a single crystal of the high-pressure modification of $NaYSi_2O_6$ (Fig. 5, Table 5).

The spectrum can be distinguished into the following high-, intermediate- and low-wavenumber regions: 800–1100, 500–800 and $<500\,\mathrm{cm}^{-1}$, respectively. In alkali and alkaline-earth metal silicates, high-intensity Raman active bands in the high-wavenumber region can be assigned to internal symmetric stretching vibrations of the non-bridging silicon–oxygen of SiO_4 groups (ν_s Si–O$^-$) [18,19]. In addition to some weak lines, we observed four bands with almost equal relative intensities around 12–38 at 968, 986, 1019 and $1058\,\mathrm{cm}^{-1}$. Previous Raman and IR studies of the cyclo-silicates benitoite ($BaTiSi_3O_9$), wadeite ($K_2ZrSi_3O_9$), Ca-walstromite ($CaSiO_3$) and α-$SrSiO_3$, all of which contain three-membered rings of silicon–oxygen tetrahedra, assigned numerous vibrational bands between

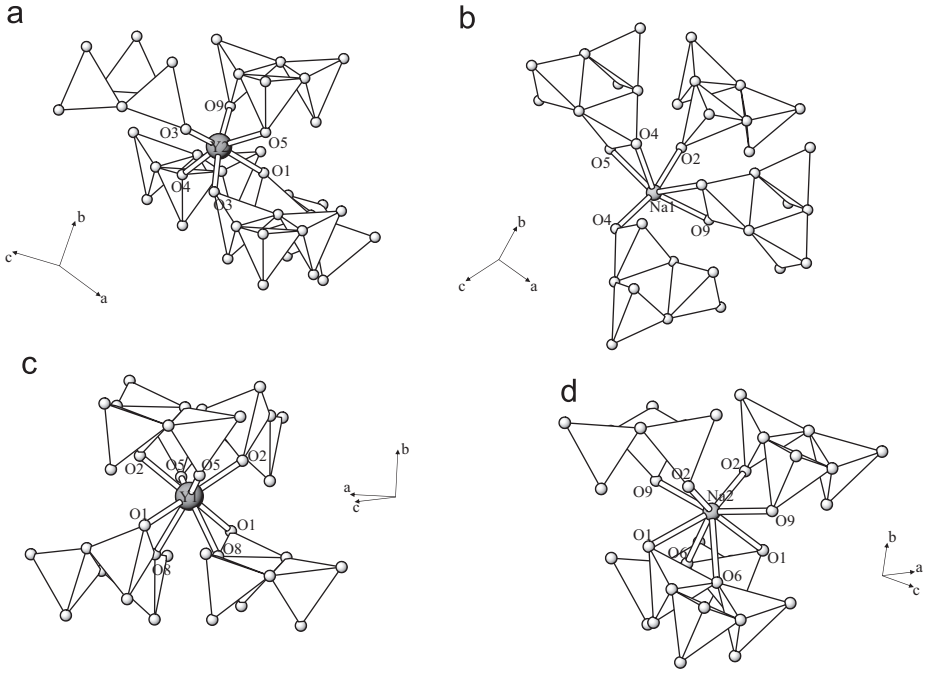

Fig. 4. Coordination environment of the four crystallographically independent non-tetrahedral cations within the structure of high-P $NaYSi_2O_6$.

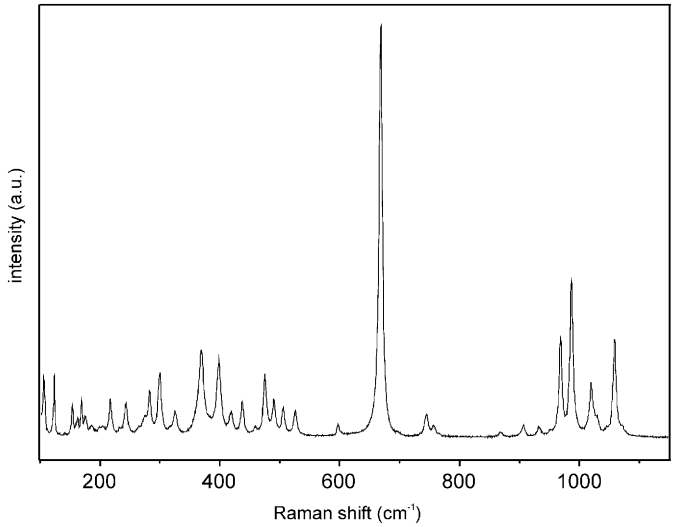

Fig. 5. Unpolarized Raman spectrum of a single crystal of high-P $NaYSi_2O_6$.

903 and 1126 cm^{-1} to ν_s Si–O^- but also to combinations of lower-wavenumber vibrational modes [20–23].

In the intermediate-wavenumber region, bending and stretching vibrations of the Si–O–Si rings (δ ring, ν ring) dominate the spectrum but also bending vibrations of the non-bridging oxygens (δSi–O^-) can be detected. Raman shift of the strongest band of the high-pressure modification of $NaYSi_2O_6$ at 667 cm^{-1} is clearly higher than comparable modes in the other cyclo-silicates with three-membered rings, which cluster around 560–600 cm^{-1} (Table 5). A negative correlation between Si–O–Si bond angles and wavenumber of bending vibrational modes was observed for sodium silicates in the range 115–165°, 900–400 cm^{-1}, respectively [18]. The mean Si–O–Si angle of the high-pressure modification of $NaYSi_2O_6$ (123.4°) is clearly lower than that of benitoite (132.9°), wadeite (133.8°) and α-$SrSiO_3$ (135.2°). In the case of Ca-walstromite (122.4°), other factors like the impact of the non-tetrahedral cations may influence the vibrational wavenumber of the bending vibration [18].

In the low-wavenumber range, vibrational modes are mainly caused by cation translations, lattice vibrations of the entire framework, ring rotations as well as deformations and δSi–O^-. Intensities of bands of the high-pressure modification of $NaYSi_2O_6$ in this region are low compared to the other cyclo-silicates with three-membered rings. This is consistent with bond valence calculations performed in this study and on the chain silicate $NaYSi_2O_6$ [6], indicating underbonding of the sodium cations in the structure.

In general, the Raman spectrum of the high-pressure modification of $NaYSi_2O_6$ is similar to that of other cyclo-silicates containing three-membered rings. The differences in Raman shifts and relative intensities can be explained by different types of weaker bonded non-tetrahedral cations, Si–O–Si bond angle variations and different arrangements of the tetrahedra in the rings.

5. Discussion and comparison with related structures

Among the large number of silicates, compounds with silicate anions exclusively based on rings of three SiO_4 tetrahedra, joined by sharing common corners are rather limited. This observation can be rationalized by the comparatively large strain of the rings which is reflected in the Si–O–Si angles. For a number of cyclo-trisilicates including minerals and synthetic phases, the corresponding individual and mean Si–O–Si angles are summarized in Table 6. It is obvious that the observed values are much lower than the value of about 140° of an unstrained Si–O–Si bond angle [24]. The present compound does not represent an exception in this sense.

Principally, two extreme configurations can be distinguished for three-membered rings of tetrahedra: (a) all tetrahedral apices point up (or down), i.e., the lateral faces of the tetrahedra in the ring are coplanar or (b) the O–O edge formed by the two terminal oxygen atoms is perpendicular to the mean plane of the ring. The maximal point group symmetries of the two configurations (assuming undistorted tetrahedra) would be $3m$ (C_{3v}) or $\bar{6}2m$ (D_{3h}), respectively. Intermediate configurations can be realized by tilting about the bridging oxygen atoms. The tilting can be numerically described by γ, the angle between the O_{term}–$O_{term.}$ vector of each tetrahedron and the direction normal to the ring plane (defined by the three Si atoms). For rings with $\bar{6}2m$ symmetry, $\gamma = 0°$, and for the other limiting situation $\gamma = \pm 35.3°$. The corresponding individual and average values realized in cyclo-trisilicate have been calculated for the published structures of Table 6 by means of a small computer program. Although the limited number of 29 structures precludes a rigorous statistical treatment of the data there is an indication that the γ-values tend to cluster in three regions. More than 50% of the listed trisilicate structures have γ-values close to or exactly equal to 0°. In this context, it has to be pointed out that $\gamma \equiv 0°$ is due to site symmetry requirements of the corresponding space groups. On the other hand, γ-values of about $\pm 35.3°$ have not been found. The largest average value that has been observed is about 25° and this value seems to be characteristic for a second group of compounds comprising a total of six structures. The third set ($\langle\gamma\rangle \sim 10°$) in turn is separated from the first two groups by distinct gaps and represents four compounds.

In the past, several groups have attempted to calculate energy-optimized geometries for rings in silicates. Therefore, it is interesting to see how the theoretically predicted results compare to the values observed in the crystal structures. Chakoumakos et al. [48], for example, selected electroneutral molecular models such as cyclo-trisiloxane $(H_2SiO)_3$ to represent silicate tetrahedral rings. According to their *ab-initio* molecular orbital study, the final optimized configuration occurs for $\gamma = 17°$. However, the calculated curve for energy versus γ-angle is very flat, indicating that this three-membered ring is flexible, covering a range of γ-values from -20 to $+20°$. Using

Table 5
Raman shifts in cm^{-1} and relative intensities (normalized to the intensity of the strongest band at $667\,cm^{-1}$) of bands in the unpolarized spectrum of high-P $NaYSi_2O_6$ and other cyclosilicates containing three-membered rings

High-P $NaYSi_2O_6$	Rel. int.	$BaTiSi_3O_9$	$K_2ZrSi_3O_9$	$Ca_3Si_3O_9$	$Sr_3Si_3O_9$	Assignments
104	14	104	107			Ring transl.[a]
122	14	112, 113	124			Cat.[b] trans., δSi–O^- (rock.[c])
139	<1					
152	7	149, 151	154, 155			Ring rot.[d], cat. trans., δ ring
160	3					
167	8				169	
173	4					
184	2					
200	2	192	192, 194			Cat. trans., ring rot., δSi–O^-, δ ring
215	8	209				δSi–O^- (rock.)
231	1	222	230			Cat. trans., δSi–O^- (rock), ring rot.
241	7	256	241			Cat. trans., ring rot.
276	4				264, 265	Lattice
281	6					
298	14				292, 294	Lattice
316	1					
324	5	337, 338, 343, 344	345	336	330	ν ring (breath.[e]), δ ring
365	7	353				δSi–O^-
368	12	361, 362, 364	372	370	363	δ ring, δSi–O^-
380	2	386	380, 381			δ ring, cat. trans.
397	17					
417	4					
436	7					
458	1	452				δ ring
473	10	467				δ ring
475	4					
489	8	493	493		488, 489	δSi–O^-
504	6			509, 510		δSi–O^-, δ ring
524	6	525			516	δSi–O^- (wagg.[f])
		565	564	556	562, 563	δSi–O^-, δ ring, ν ring
596	2		586, 588	578		δSi–O^-
		628	610, 632			δ ring, ν ring (breath), δSi–O^-
667	100					
744	5	736	736, 740			δ ring, δSi–O^- (wagg.)
756	2	754				δSi–O^- (wagg.)
868	1					
906	2	903			910	ν Si–O^-
		917, 926	916			ν Si–O^-
932	2	938	932	933		ν Si–O^-
952	1					
962	1					
968	23		973		965, 966	ν Si–O^-
986	38	993	992	982		ν Si–O^-
1019	12		1010			Combination?
1028	3					
1036	1					
1046	1	1048			1043, 1044	ν ring
1058	23		1057			Combination
1069	2	1087		1076, 1077		ν ring

[a]Translation.
[b]Cation.
[c]Rocking.
[d]Rotation.
[e]Breathing.
[f]Wagging.

$[(OH)_2SiO]_3$ molecules for the optimization, the same authors obtained a completely different result: a single energy minimum was now found for $\gamma = 0^\circ$. Indeed, this value is realized for a larger number of structures, but this model calculation cannot explain the occurrence of the other γ-values observed in trisilicate clusters. A possible explanation for the discrepancies between prediction and experiment is obvious: the choice of neutral tetrahedral

Table 6
Summary of silicates exclusively based on $[Si_3O_9]$ anions

Compound	Range of Si–O–Si angles; ⟨Si–O–Si⟩ (deg)	Range of tilt angles γ; ⟨γ⟩ (deg)	Reference
Benitoite ($BaTiSi_3O_9$)*	132.9	0.0; 0.0	[25]
Pabstite ($Ba(Sn_{0.77}Ti_{0.23})Si_3O_9$)*	132.8	0.0; 0.0	[26]
Bazirite ($Ba(Zr_{0.97}Ti_{0.03})Si_3O_9$)*	132.7	0.0; 0.0	[26]
$BaSiSi_3O_9$*	133.7	0.0; 0.0	[27]
Wadeite ($K_2ZrSi_3O_9$)$^{\$}$	133.8	0.0; 0.0	[28]
$K_2TiSi_3O_9^{\$}$	135.4	0.0; 0.0	[29]
$K_2SiSi_3O_9^{\$}$	134.5	0.0; 0.0	[30]
$K_2SnSi_3O_9^{\$}$	133.7	0.0; 0.0	[31]
$Rb_2TiSi_3O_9^{\$}$	135.7	0.0; 0.0	[31]
$Rb_2SnSi_3O_9^{\$}$	136.9	0.0; 0.0	[31]
$CsZrSi_3O_9^{\$}$	136.6	0.0; 0.0	[29].
$Na_2Be_2Si_3O_9$	131.3–136.5; 133.2	0.0; 0.0	[32]
$La_3F_3[Si_3O_9]$	134.2	0.0; 0.0	[33]
$Cs_5AgSi_3O_9$	133.0–137.7; 134.7	0.0; 0.0	[34]
$Cs_8Nb_{10}O_{23}(Si_3O_9)_2$	136.0	0.0; 0.0	[35]
Pseudo-wollastonite (α-$CaSiO_3$)	134.5–134.8; 134.6	0.5–0.8; 0.6	[36]
α-$SrSiO_3$	135.0–135.6; 135.2	2.4–2.6; 2.5	[37]
Catapleiite ($Na_2ZrSi_3O_9 \cdot 2H_2O$)	134.4–134.7; 134.6	2.1–2.5; 2.3	[38]
$Ca_3Y_2(Si_3O_9)_2$	133.6–133.9; 133.8	5.2–8.5; 6.7	[39]
Ca-catapleiite ($CaZrSi_3O_9 \cdot 2H_2O$)	132.6–133.2; 133.0	7.8–8.9; 8.2	[40]
$K_6Si_3O_9^{\S}$	130.8–133.3; 132.1	8.6–16.5; 12.8	[41]
$Rb_6Si_3O_9^{\S}$	133.2–134.3; 133.8	8.2–13.8; 11.1	[42]
$Cs_6Si_3O_9^{\S}$	133.8–134.9; 134.4	6.8–10.7; 8.9	[42]
$BaNaNdSi_3O_9$	125.4–125.8; 125.5	17.5–22.7; 20.9	[43]
Walstromite ($BaCa_2Si_3O_9$)$^{\#}$	120.3–126.1; 124.5	22.1–28.2; 25.8	[44]
Margarosanite ($PbCa_2Si_3O_9$)$^{\#}$	120.0–123.2; 121.7	21.1–27.4; 25.3	[45]
Ca-walstromite ($CaSiO_3$)$^{\#}$	121.3–125.0; 122.4	22.4–26.9; 25.4	[46]
Wollastonite-II (δ-$CaSiO_3$)	122.9–124.0; 123.4	22.4–26.9; 25.3	[47]
High-P $NaYSi_2O_6$	122.1–124.3; 123.4	21.2–28.2; 24.2	This work

Compounds marked with the same superscript sign are isostructural.

trimers for the simulation neglects possible influences of the surrounding non-tetrahedral cations. A more realistic approach should be based on $[SiO_3]_3$ groups and include a description of the ionic environment that is needed for charge compensation, i.e., the first cation shell surrounding the ring.

Up to a certain level $NaYSi_2O_6$ and $CaSiO_3$ exhibit similar features. Like in $NaYSi_2O_6$, increasing pressure induces phase transformations in monocalcium silicate from a single chain structure (β-$CaSiO_3$ or wollastonite) to structures based on $[Si_3O_9]$ rings (walstromite-type $CaSiO_3$, δ-$CaSiO_3$ or wollastonite-II). Furthermore, the ring configurations and γ-values of the high-P polymorphs of both compounds are almost the same (see Table 6). Nevertheless, the stacking of rings is different, indicating that high-P $NaYSi_2O_6$ is not a new member of the walstromite family but represents an own new structure type.

Finally, we would like to compare the two polymorphic forms of $NaYSi_2O_6$ briefly. From a structural point of view both modifications differ considerably. Whereas the ambient pressure form belongs to the group of *vierer* single chain silicates, the high-P polymorph is based on cyclic three-membered rings of $[SiO_4]$ tetrahedra. The comparison of the calculated densities of the ambient pressure modification ($\rho = 3.32\,g/cm^3$) and the present quenched high-P polymorph ($\rho = 3.55\,g/cm^3$) follows the expected trend. The electrostatic or Madelung part of the lattice energy was calculated for both modifications using the program MAPLE [49]. The resulting values for the ambient and high-pressure form are 40 154 and 39 108 kJ/mol, respectively. Since this Coulomb term represents the most important part of the total lattice energy, this result can be used as energetic indication why the formation of chain silicate is preferred at ambient pressure.

6. Concluding remarks

As already mentioned in the introduction, the compounds belonging to the series $NaXSi_2O_6$ (*X*:Y, Sc, Ti, Al, V, Cr, In, Fe, Ga) adopt tetrahedral chain structures at ambient pressure with chain periodicities of two and four, respectively. So far, $NaYSi_2O_6$ is the only example of the series where the presence of a ring silicate has been described (at least at elevated pressures). In order to find further possible candidates where a ring silicate may be observed at high-P, one could focus on the following two parameters: the ionic radius and the electronegativity. In addition to the valence of an additional guest cation in a silicate, these two parameters are of special importance and will greatly influence the topology that is adopted by a structure [24]. Unfortunately, the databases for the ionic radii [50] and the electronegativities [51] indicate that the

size of Y^{3+} (for an eight-fold coordination: $r = 1.019$ Å) and its electronegativity (1.22) are significantly different from the values for the other *X*-cations. With this respect, Sc^{3+} would be the closest related cation of the series. However, if one extends the search to the lanthanides it becomes obvious that the trivalent cations of holmium and dysprosium almost perfectly match the requirements concerning size and electronegativity. Therefore, the compositions $NaHoSi_2O_6$ and $NaDySi_2O_6$ would be interesting candidates for high-P synthesis experiments.

References

[1] G.J. Redhammer, H. Ohashi, G. Roth, Acta Crystallogr. B 59 (2003) 730–746.
[2] K.A. Gscheidner, J. Less-Common Met. 25 (1971) 405–422.
[3] C. Frondel, Z. Kristallogr. 127 (1968) 121–138.
[4] F.J. Cervantes Lee, Ph.D. Thesis, University of Aberdeen, 1981.
[5] G.J. Redhammer, G. Roth, Acta Crystallogr. C 59 (2003) i120–il24.
[6] D. Többens, V. Kahlenberg, R. Kaindl, Inorg. Chem. 44 (25) (2005) 9554–9560.
[7] F.R. Boyd, J.L. England, J. Geophys. Res. 65 (1960) 741–748.
[8] M.C. Burla, M. Camalli, B. Carrozzini, G.L. Cascarano, C. Giacovazzo, G. Polidori, R. Spagna, J. Appl. Crystallogr. 36 (2003) 1103.
[9] A.J.C. Wilson (Ed.), International Tables for Crystallography, vol. C, Kluwer Academic Publishers, Dordrecht, The Netherlands, 1995.
[10] G.M. Sheldrick, SHELX97—Programs for Crystal Structure Analysis (Release 97-2), University of Göttingen, Germany, 1998.
[11] E. Dowty, ATOMS Version 5.1, Shape Software, 2000.
[12] K. Robinson, G.V. Gibbs, P.H. Ribbe, Science 172 (1971) 567.
[13] N.N. Brese, M. O'Keeffe, Acta Crystallogr. B 47 (1991) 192–197.
[14] E. Dowty, VIBRATZ Version 2.1, Shape Software, 2000.
[15] M.I. Aroyo, A. Kirov, C. Capillas, J.M. Perez-Mato, H. Wondratschek, Acta Crystallogr. A 62 (2006) 115–128.
[16] M.I. Aroyo, J.M. Perez-Mato, C. Capillas, E. Kroumova, S. Ivantchev, G. Madariaga, H. Kirov, H. Wondratschek, Z. Kristallogr. 221 (2006) 15–27.
[17] E. Kroumova, M.I. Aroyo, J.M. Perez-Mato, A. Kirov, C. Capillas, S. Ivantchev, H. Wondratschek, Phase Transitions 76 (2003) 155–170.
[18] J.-L. You, G.-C. Jiang, H.-Y. Hou, H. Chen, Y.-Q. Wu, K.-D. Xu, J. Raman Spectrosc. 36 (2005) 237–249.
[19] M. Akaogi, N.L. Ross, P. McMillan, A. Navrotsky, Am. Mineral. 69 (1984) 499–512.
[20] D.A. McKeown, M.I. Bell, C.C. Kim, Phys. Rev. B 48 (1993) 16357–16365.
[21] D.A. McKeown, A.C. Nobles, M.I. Bell, Phys. Rev. B 54 (1996) 291–304.
[22] M. Handke, M. Sitarz, W. Mozgawa, J. Mol. Struct. 450 (1998) 229–239.
[23] M. Sitarz, W. Mozgawa, M. Handke, J. Mol. Struct. 404 (1997) 193–197.
[24] F. Liebau, Structural Chemistry of Silicates, Springer, Berlin, 1985.
[25] K. Fischer, Z. Kristallogr. 129 (1969) 222–243.
[26] F.C. Hawthorne, N. Jb. Mineral. Monatsh. (1987) 16–30.
[27] L.W. Finger, R.M. Hazen, B.A. Fursenko, J. Phys. Chem. Solids 56 (1995) 1389–1393.
[28] K. Sakai, T. Nakagawa, M. Okuno, K. Kihara, J. Mineral. Petrol. Sci. 95 (2000) 24–31.
[29] H. Xu, A. Navrotsky, M.L. Balmer, Y. Su, Phys. Chem. Miner. 32 (2005) 426–435.
[30] D.K. Swanson, C.T. Prewitt, Am. Mineral. 68 (1983) 581–585.
[31] J. Choisnet, A. Deschanvres, B. Raveau, J. Solid State Chem. 7 (1973) 408–417.
[32] D. Ginderow, F. Cesbron, M.C. Sichere, Acta Crystallogr. B 38 (1982) 62–66.
[33] H. Müller-Bunz, T. Schleid, Z. Anorg. Allg. Chem. 625 (1999) 1377–1383.
[34] A. Möller, P. Amann, Z. Anorg. Allg. Chem. 627 (2001) 172–179.
[35] M.P. Crosnier, C. Pagnoux, D. Guyomard, A. Verbaere, Y. Piffard, M. Tournoux, Eur. J. Solid State Inorg. Chem. 28 (1991) 971–981.
[36] H. Yang, C.T. Prewitt, Am. Mineral. 84 (1999) 1902–1905.
[37] F. Nishi, Acta Crystallogr. C 53 (1997) 534–536.
[38] V.V. Ilyukhin, A.A. Voronkov, N.N. Nevskii, N.V. Belov, Dokl. Akad. Nauk SSSR 260 (1981) 623–627 (in Russian).
[39] H. Yamane, T. Nagasawa, M. Shimada, T. Endo, Acta Crystallogr. C 53 (1997) 1533–1536.
[40] S. Merlino, M. Pasero, M. Bellezza, D.Yu. Pushcharovsky, E.R. Gobetchia, N.V. Zubkova, I.V. Pekov, Can. Mineral. 42 (2004) 1037–1045.
[41] R. Werthmann, R. Hoppe, Rev. Chim. Miner. 18 (1981) 593–607.
[42] C. Hoch, C. Roehr, Z. Naturforsch. B 56 (2001) 423–430.
[43] Yu.A. Malinovskii, O.S. Bondareva, S.V. Baturin, Dokl. Akad. Nauk. SSSR 275 (1984) 372–375 (in Russian).
[44] L.S. Dent Glasser, F.P. Glasser, Am. Mineral. 53 (1968) 9–13.
[45] R.L. Freed, D.R. Peacor, Z. Kristallogr. 128 (1969) 213–228.
[46] W. Joswig, E.F. Paulus, B. Winkler, V. Milman, Z. Kristallogr. 218 (2003) 811–818.
[47] F. Trojer, Z. Kristallogr. 130 (1969) 185–206.
[48] B.C. Chakoumakos, R.J. Hill, G.V. Gibbs, Am. Mineral. 66 (1981) 1237–1249.
[49] R. Hübenthal, MAPLE, Program for the Calculation of MAPLE-Values, Version 4, University of Gießen, 1993.
[50] R.D. Shannon, Acta Crystallogr. A 32 (1976) 751–767.
[51] L. Pauling, The Nature of the Chemical Bond, third ed., Cornell University Press, Ithaka, NY, 1967.